

## Development of an embedded-atom potential for a bcc metal: Vanadium

James B. Adams\* and Stephen M. Foiles

*Theoretical Division, Sandia National Laboratories, P.O. Box 969, Livermore, California 94551-0969*

(Received 17 April 1989)

An empirical embedded-atom potential for a bcc metal (vanadium) has been developed by fitting the embedding function, electron density, and pair interaction to the lattice constant, cohesive energy, elastic constants, and vacancy-formation energy. This potential has been used to calculate vacancy and divacancy properties, interstitial properties, thermal expansion, bulk-phonon dispersion, surface relaxation, surface energy, and liquid volume; in all cases the calculations are in reasonable agreement with experiment.

### I. INTRODUCTION

Atomistic simulations are becoming an increasingly powerful tool for studying the structure and properties of materials. Simulation methods fall into two classes, the *ab initio* or first-principles methods, and the (semi)empirical methods. The *ab initio* methods involve solving Schrödinger's equation with various degrees of approximation; these techniques are generally limited to very small systems (less than a few dozen atoms).

The (semi)empirical methods are capable of treating much larger systems (thousands to millions of atoms), but their success is limited by the reliability of their potentials. Pair potentials have previously been popular for metals, but they suffer from two major errors: the vacancy-formation energy is always the same as the cohesive energy, and  $C_{12} = C_{44}$ . These errors can be overcome by including a volume-dependent energy term, but the volume-dependent term is poorly defined at surfaces.

To overcome the limitations of pair potentials, Daw and Baskes<sup>1</sup> developed a model of metallic cohesion known as the embedded-atom method (EAM). It is more general than pair potentials, in that it involves many-body interactions. The EAM is based on density-functional theory, which asserts that the energy of a material can be written as a unique functional of the electron density. In the EAM, the important aspect of the electron density is assumed to be the local electron density at each atomic site, as provided by the surrounding atoms. The total energy is divided into an electrostatic interaction plus an embedding energy, which is the energy required to place an atom in a uniform electron gas. Thus, the total energy of an arbitrary arrangement of atoms is given by

$$E_{\text{tot}} = \sum_i F_i(\rho_{h,i}) + \frac{1}{2} \sum_{\substack{i,j \\ (i \neq j)}} \phi_{ij}(R_{ij}), \quad (1)$$

where  $F_i(\rho)$  is the embedding energy of atom  $i$ ,  $\rho_{h,i}$  is the host electron density at atom  $i$  due to the surrounding atoms,  $\phi_{ij}(R_{ij})$  is a short-ranged electrostatic interaction between atom  $i$  and atom  $j$ ,  $R_{ij}$  is the distance between atoms, and the sums are over all atoms. The host elec-

tron density is approximated by the superposition of atomic electron densities.

Daw<sup>2</sup> recently derived the EAM form from density-functional theory, and thereby obtained the EAM functions. Although these functions do not represent the actual metals as accurately as empirical functions, they clearly demonstrate the physical origin of the terms in Eq. (1). His derivation ignores band-structure effects and assumes that the electron density can be approximated by a superposition of atomic electron densities. Both of these assumptions are better approximations for fcc metals than for bcc metals, suggesting that EAM-type models are less appropriate for bcc metals. Jacobson, Norskov, and Puska<sup>3</sup> have also derived EAM-type functions from *ab initio* methods, and their results also suggest that the EAM-type approach might be inappropriate for bcc metals.

Accurate empirical functions for the fcc metals (Ag, Au, Cu, Ni, Pd, Pt) and their alloys were developed by Foiles, Baskes, and Daw (FBD) (Ref. 4) by fitting both  $F_i(\rho)$  and  $\phi_{ij}(R_{ij})$  to the bulk lattice constant, sublimation energy, elastic constants, vacancy-formation energy, and alloy heat of mixing. Other EAM functions have also been developed,<sup>1,5-10</sup> but the FBD functions are the most commonly used. The EAM has been shown to accurately reproduce many physical properties, such as vacancy and interstitial properties,<sup>4</sup> phonon dispersion,<sup>11</sup> liquid-metal structure,<sup>5</sup> alloys,<sup>4</sup> bulk diffusion in metals and alloys,<sup>6,12</sup> thermal expansion,<sup>13,14</sup> Gibb's free energies,<sup>13</sup> and the structure of grain boundaries.<sup>15,16</sup> They have also been fairly successful in describing many properties of surfaces, including surface energies and relaxations,<sup>4</sup> surface reconstructions,<sup>9,17,18</sup> surface segregation,<sup>7,19</sup> and phonon dispersion at surfaces.<sup>20,21</sup> The ability of the EAM to accurately describe such a wide range of properties is one of the most surprising and powerful justifications of the approach.

Other researchers have used similar approaches to develop many-body potentials, but they generally replace the atomic electron density with a parametrized function which has an exponential-like decay. Using this quasi-electron-density approach, Voter and Chen<sup>22</sup> developed functions for the fcc metals, and Oh and Johnson<sup>10</sup> developed simplified EAM functions for fcc and hcp metals. Baskes has proposed modified EAM potentials for

covalently bonded materials (Si and Ge) by including a directionally dependent term in the quasi-electron density to approximate the covalent bonding between atoms.<sup>23,24</sup>

However, previous attempts to develop accurate models for bcc metals have generally met with only limited success. Finnis and Sinclair (FS) (Ref. 25) used a mathematically similar formalism to develop potentials for the bcc metals, although they use a different embedding function due to a different physical motivation. Their potentials describe the elastic constants,<sup>25</sup> phonon dispersion,<sup>26</sup> and simple defect properties.<sup>27–29</sup> Two modifications of the FS potentials have been proposed to correct unphysical behavior at close interatomic separations, namely the pressure versus volume relation.<sup>27,30</sup> (The EAM functions have the correct pressure versus volume relation, since they were fitted to an accurate equation of state<sup>32</sup>—see the Appendix).

Marchese, Jacucci, and Flynn<sup>32</sup> have shown that the FS potentials (including the modified ones<sup>27,30</sup>) predict thermal expansions that are too low and in many cases negative. This flaw implies that the third derivatives of the FS potentials are incorrect, so that the FS potentials may be inaccurate for large distortions of the perfect crystal lattice.

Johnson and Oh<sup>33</sup> and Eridon<sup>34</sup> have developed EAM-like potentials for the bcc metals, and achieved good fits to the experimental data. Although these approaches are promising, to the best of our knowledge the predictive power of these potentials has not yet been tested.

The purpose of this paper is to develop and thoroughly test EAM functions for the bcc metals. We will begin with a single element, vanadium. This element proved to be one of the most intractable to the FS approach (it had a negative thermal expansion, and it required major modifications to its short-range interaction. Potentials for the other bcc metals will be developed in the future with the same formalism.

Self-consistent local-density-functional calculations of the electron density in bulk bcc and fcc transition metals indicate that the superposition of atomic electron densities is a better approximation in the fcc metals than in the bcc metals.<sup>35</sup> Therefore, we will allow the electron density to be an adjustable function. Our approach is virtually identical to that taken by Voter and Chen<sup>22</sup> in developing functions for the fcc metals; the primary differences are that we use a different cutoff condition for the functions, and we only weakly fit to the dimer properties (see Sec. II).

Section II discusses the development of  $F^{\text{VAN}}$ , an EAM potential for vanadium. Section III discusses the calculations carried out with  $F^{\text{VAN}}$  to fully test its reliability and range of applicability. Finally, Sec. IV summarizes the results.

The Appendix presents a simple calculation of the pressure versus volume relation of the equation of state used in the EAM.

## II. DEVELOPMENT OF AN EAM FUNCTION FOR VANADIUM

Our previous attempts to develop potentials for the bcc metals assumed that the electron density is given by a su-

perposition of atomic electron densities; however, these attempts were unsuccessful. Since the electron density in bcc metals is less well approximated by the superposition of atomic densities than in the fcc metals, we have instead followed Voter and Chen's approach<sup>8,22</sup> of using an adjustable electron density which has a reasonable form (that of a  $4s$  orbital). This form of the density does not include the directional dependence of the  $d$ -like states; it was chosen simply because spherically symmetric electron densities are easier to incorporate in the model. Baskes<sup>23</sup> has recently proposed a modified embedded-atom method for silicon which includes directionally dependent electron densities to approximately treat covalent bonding. This approach provides a better description of silicon than one based on spherical densities and such an approach might increase the accuracy of functions for bcc metals. However, it is still an unanswered question whether simply including a better description of the electron density will be sufficient to obtain a good description of the energetics of materials where covalent effects are important. Despite the possible inaccuracies of assuming spherically symmetric electron densities, it will be seen that our simple approach is reasonably successful in describing the behavior of vanadium.

Voter gave a thorough explanation of his approach previously,<sup>8,22</sup> so we will merely mention the major points here. The pair term in Eq. (1) is assumed to have the form of a Morse potential:

$$\Phi(r) = D_m (e^{-2\alpha(r-r_m)} - 2e^{-\alpha(r-r_m)}) \quad (2)$$

$D_m$  is the depth of the minimum,  $r_m$  is the separation at the minimum, and  $\alpha$  determines the curvature near the minimum. Each atom's contribution to the total electron density is given by  $\rho(r)$ :

$$\rho(r) = r^6 (e^{-\beta r} + 512e^{-\gamma r}), \quad (3)$$

where  $\beta$  and  $\gamma$  are adjustable parameters. The first term represents the density of a  $4s$  orbital, and the second term is added to ensure that the electron density decreases with  $r$  over the range of relevant interaction distance (the preexponential value of 512 is the relative normalization factor). The second term may be thought of as the contribution of core electrons. It should be noted that Voter required that  $\gamma$  have exactly the value of  $2\beta$ , whereas we treat it as an adjustable parameter; this means that the 512 term is no longer the correct normalization factor, but simply an additional parameter which we keep constant for simplicity's sake. Although allowing  $\gamma$  to vary is not absolutely necessary, it seemed to slightly improve the fit of the functions.

Following Foiles *et al.*,<sup>4</sup> the EAM function  $F(\rho_i)$  is specified by requiring that the total cohesive energy [Eq. (1)] be exactly equal to the universal equation of state determined by Rose *et al.*<sup>31</sup> This equation of state releases the total energy of the system to its lattice constant, and ensures that the functions have a correct pressure versus volume relationship. The purpose of fitting  $F(\rho_i)$  in this manner is to ensure that the function behaves properly over a large range of densities and to in-

corporate the overall anharmonicity of the cohesive energy.

Since the above functional form for the EAM function  $F$  continues out to infinity, it is necessary to cut  $F$  off at some distance  $r_{\text{cut}}$ . We follow the approach taken by Foiles *et al.*,<sup>4,7</sup> which they unfortunately neglected to mention in their paper. We will now present their approach.

The embedding function is determined by requiring that the zero-temperature equation of state<sup>31</sup>  $E(a)$  is satisfied for all lattice constants  $a$ . However, if this is taken literally, as the lattice is expanded to the point where the nearest-neighbor distance  $R_{\text{NN}}$  is equal to  $r_{\text{cut}}$ , the density and pair interaction will be zero but the total energy is not. This means that the embedding function at zero density is nonzero and the functions will not reasonably handle the case of an atom moving away from the solid. To handle this, the equation of state was modified so that  $E(a_{\text{cut}}) = 0$ , where  $a_{\text{cut}}$  is the lattice constant such that the nearest-neighbor distance equals  $r_{\text{cut}}$ , i.e.,  $a_{\text{cut}} = \sqrt{2}r_{\text{cut}}$  for a fcc lattice. The modified equation of state is defined by the following equations:

$$E(a) = E_{\text{sub}} \frac{f(a^*) - e}{1 - e},$$

where  $E_{\text{sub}}$  is the sublimation energy, and

$$f(a^*) = 1(1 + a^*)e^{-a^*},$$

$$a^* = \frac{a - a_0}{\lambda_0}.$$

$a_0$  is the equilibrium lattice constant, and the other parameters are given by

$$e = f((r_{\text{cut}} - R_{\text{NN}})/(\lambda_0 R_{\text{NN}})),$$

$$\lambda_0 = \left[ \frac{E_{\text{sub}}}{9B\Omega} \right]^{1/2},$$

$$\lambda = \frac{\lambda_0}{\sqrt{1 - e}}.$$

The net result of the above equations is that  $E(a)$  is not changed near  $a = a_0$  [through second order in  $(a - a_0)$ ] but that  $E(a)$  goes to zero near  $a = a_{\text{cut}}$ . Note that for the cutoff distance used,  $e$  is fairly small (0.115), which is approximately a 10% correction.

The functional forms for  $\rho$  and  $F$  given above continue out to infinity, so it is necessary to cut them off at some distance  $r_{\text{cut}}$ . To ensure that the functions are suitable for atomistic simulations, we require that the functions and their first derivatives are equal to zero at  $r_{\text{cut}}$ . Voter used a form given by

$$f_{\text{smooth}}(r) = f(r) - f(r_{\text{cut}}) + \frac{r_{\text{cut}}}{m} \left[ 1 - \left( \frac{r}{r_{\text{cut}}} \right)^m \right] \left[ \frac{df(r)}{dr} \right]_{r=r_{\text{cut}}}, \quad (4)$$

where  $m = 20$ . We instead chose this form with  $m = 1$ , so that the functions would be cut off more gradually; our simplified expression for the cutoff procedure is thus

$$f_{\text{smooth}}(r) = f(r) - f(r_{\text{cut}}) + (r_{\text{cut}} - r) \left[ \frac{df(r)}{dr} \right]_{r=r_{\text{cut}}} \quad (5)$$

Using the above cutoff procedure, the functions were found to be fairly insensitive to the cutoff distance, and we finally chose a value halfway between third- and fourth-nearest neighbors (see Table I). This form for the cutoff does significantly change the shape of the functions (see Figs. 1 and 3), and we found that this form was important to the success of our approach; the use of other cutoff procedures (including Voter's) were generally not successful. Interestingly enough, values of  $m = 2$  to  $m = 4$  were moderately successful, but the choice of  $m = 1$  seems best. This suggests that a more general form for both  $\rho$  and  $F$  would be better, and allow a much wider choice of cutoff procedures.

### A. Fitting procedure

Given the above expressions for  $\rho$ ,  $\Phi$ , and  $F$ , we will now discuss how the functions were fit to experimental data. Due to the way the embedding function  $F$  is determined, the fit to the lattice constant, cohesive energy, and bulk modulus is exact for any choice of  $\rho$  and  $\Phi$ . The six parameters  $R_m$ ,  $D_m$ ,  $\alpha$ ,  $\beta$ ,  $\gamma$ , and  $r_{\text{cut}}$  in Eqs. (2)–(4) are determined by searching parameter space to minimize the difference between calculated and experimental values of the shear moduli [ $G = (C_{11} - C_{12})/2$  and  $C_{44}$ ], vacancy-formation energy ( $E_v^f$ ), bcc-fcc phase stability, dimer bond energy ( $D_e$ ), and dimer bond length ( $R_e$ ). The

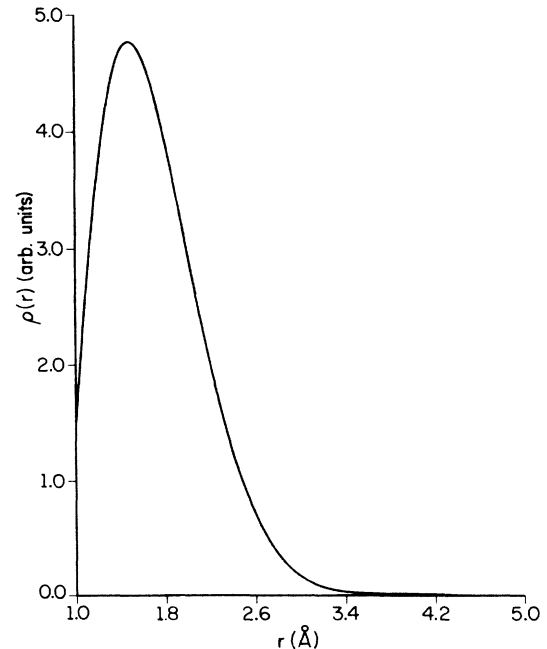


FIG. 1. The quasidelectron densities  $\rho(r)$  for  $F^{\text{VAN}}$ , in arbitrary units.

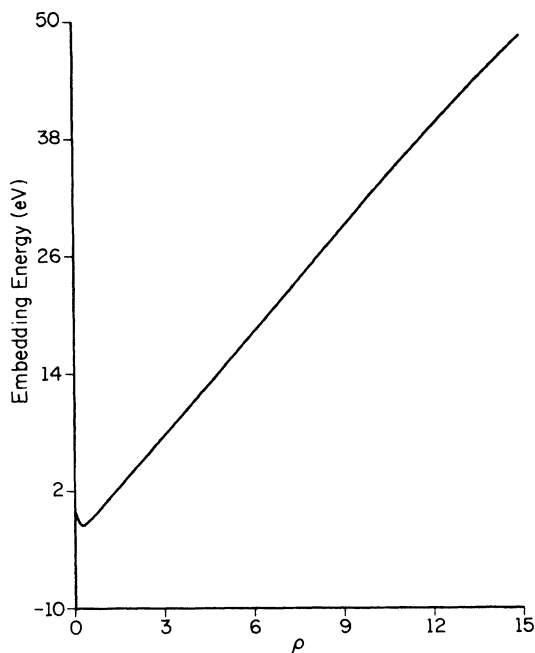


FIG. 2. The EAM embedding function  $F(\rho)$ , in units of eV. The total electron density at an atom in a perfect crystal, as contributed by other atoms, is 6.114 (arbitrary units).

searching algorithm iteratively adjusts the choice of initial parameters so as to find the local minimum in parameter space.

Using different guesses of the initial values of the pa-

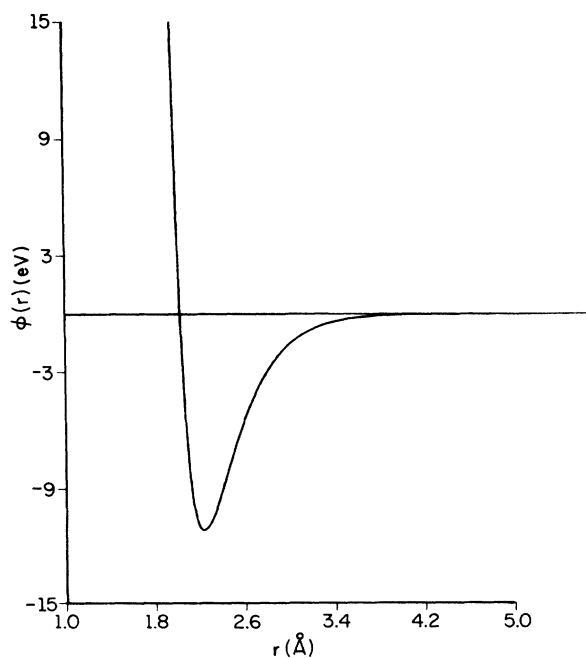


FIG. 3. The pair potential  $\phi(r)$  in units of eV. This potential is a Morse potential, modified by a cutoff term.

TABLE I. Parameters which describe the fit for  $F^{VAN}$ .

Parameter	Value
$D_m$ (eV)	11.229 933 7
$\alpha$ ( $\text{\AA}^{-1}$ )	3.418 491 6
$r_m$ ( $\text{\AA}$ )	2.231 861 9
$\beta$ ( $\text{\AA}^{-1}$ )	1.862 836 8
$\gamma$ ( $\text{\AA}^{-1}$ )	4.320 001 9
$r_{\text{cut}}$ ( $\text{\AA}$ )	4.65

rameters, many reasonable fits to the above bulk material properties were found. However, in no case could the dimer bond energy and bond length be accurately fitted while still fitting the other experimental data. This is in contrast to Voter's functions for the fcc metals,<sup>8</sup> which fit both bulk and dimer properties.

Since dimer properties could not be fitted accurately, their relative importance in the fitting procedure was reduced by an order of magnitude. Similarly, since the exact value of the bcc-fcc phase stability is not well known we simply required that it be positive.

Many sets of parameters were found to yield very good fits to the bulk data (within a few percent), so these functions were tested further to determine which were the best. We decided to primarily investigate thermal expansion and vacancy migration. There were several reasons for this choice. First, there is reliable experimental data for both of these properties (especially for thermal expan-

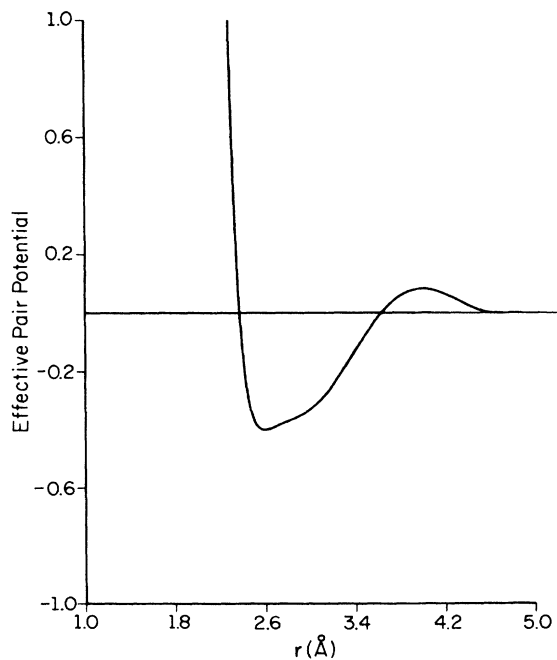


FIG. 4. The effective pair potential,  $\phi_{\text{eff}}(r)$  in units of eV. The potential is determined by summing  $[\phi_{\text{eff}}(r)]_{ij}$  and an approximation for  $F(\rho)$ , where  $F(\rho)$  is approximated with a Taylor-series expansion about the equilibrium electron density (Ref. 5).

sion). Secondly, whereas the elastic constants are related to second derivatives of the crystal energy, thermal expansion is related to third derivatives of the crystal energy. Finally, vacancy migration involves a nonuniform distortion of the lattice and atomic separations closer than those which enter the other bulk properties used here. These two criteria were used to determine which of the many vanadium functions was the best, and that function was then used to determine several other material properties.

Surprisingly, many of the functions which yielded good fits to the elastic constants and vacancy-migration energy did a very poor job at predicting thermal expansion and/or the vacancy-migration energy. Many of the functions yielded low or even negative thermal expansions, and often too low a vacancy-migration energy. This is similar to the FS functions,<sup>25,27,30</sup> which had very low (or negative) thermal expansions<sup>32</sup> and usually somewhat low vacancy-migration energies.<sup>28,29</sup> A few functions were found which yielded too high a vacancy-migration energy or thermal expansion, but this was rare. Thermal expansion and vacancy-migration energy appeared to be largely uncorrelated; often one value would be correct and the other would be too high or too low.

Thus, thermal expansion and vacancy-migration energy appear to be two stringent and largely uncorrelated tests of the functions. Simply fitting the lattice constants, cohesive energy, lattice constants, and vacancy-formation energy is not sufficient for developing good functions for the bcc metals with this formalism. Using these two stringent criteria, we selected one function,  $F^{\text{VAN}}$ , for fur-

ther studies. The parameters which describe  $F^{\text{VAN}}$  are listed in Table I. It should be noted that the cutoff distance,  $r_{\text{cut}}$ , is almost exactly halfway between third- and fourth-nearest neighbors,  $\rho$ ,  $\Phi$ , and  $F$  are graphed in Figs. 1–3. In Fig. 4 we graph the effective pair potential, which is determined by modifying  $F$  by approximating the effect of the embedding function with its first and second derivatives at the equilibrium separation distance.<sup>5</sup> This pair-potential approximation of the EAM interactions yields some insight into their properties.

Table II compares the calculations using  $F^{\text{VAN}}$  and the experimental data to which it was fitted. Due to the form of the embedding function, the lattice constant, sublimation energy, and bulk modulus are fitted exactly. In general, the fit to the experimental data is quite good, with the exception of dimer properties, which appear to be beyond the capabilities of this simple model.

### III. RESULTS

The previous section described the development of a function for vanadium by fitting to various material properties. In this section we first discuss thermal expansion and vacancy properties, which were used to determine which of many vanadium functions was the most reliable. Then, we used that function,  $F^{\text{VAN}}$ , to predict many other properties, including divacancy properties, interstitial properties, phonon dispersion, surface energies, surface relaxations, and liquid volume.

#### A. Thermal expansion

A detailed discussion of thermal expansion was given in a previous paper,<sup>16</sup> so we will merely highlight the major points here. At temperatures below the Debye temperature (about 380 K for vanadium<sup>37</sup>), quantum effects are important in determining thermal expansion. Specifically, certain phonon modes will be “frozen out,” and also zero-point phonon vibrations are significant.

Above the Debye temperature, quantum effects become unimportant, and thermal expansion may be determined from classical calculations, such as molecular dynamics (MD). Thermal expansion is due to anharmonic terms in the cohesive energy for small displacements of the atom about its equilibrium position at 0 K. Thus, thermal expansion is related to third derivatives of the cohesive energy near the 0-K equilibrium position. (Remember that the elastic constants are related to the second derivatives.)

Using MD techniques, we calculate the average lattice constant at 500, 1000, 1500, and 2000 K at zero pressure. In Fig. 5, we compare the thermal expansion of  $F^{\text{VAN}}$  with experiment.<sup>40</sup> The theoretical results have been normalized to  $a_{\text{QH}}^0 = 3.0517 \text{ \AA}$ , the lattice constant at 0 K as calculated from the quasiharmonic (QH) approximation. The QH calculations include the effect of zero-point vibrations.<sup>16</sup>

The agreement with experiment is good, especially when one realizes that the calculated curve will approach 0 at 0 K once the quantum effects are properly included. The calculated curve is almost linear, whereas the experi-

TABLE II. Pure metal properties used to fit  $F^{\text{VAN}}$ : equilibrium lattice constants, sublimation energy, bulk modulus, elastic constants, and vacancy-formation energy. The bcc phase stability, dimer bond energy, and dimer bond length were only weakly included in the fit. Where two values are given, the top value represents the calculated value with  $F^{\text{VAN}}$ , and the bottom value represents the experimental value.

$a_0$ (Å)	3.038 <sup>a</sup>
$E_{\text{sub}}$ (eV)	5.30 <sup>b</sup>
$B$ ( $10^{12}$ ergs/cm <sup>3</sup> )	1.57 <sup>a</sup>
$C_{11}$ ( $10^{12}$ ergs/cm <sup>3</sup> )	2.32
	2.29 <sup>a</sup>
$C_{12}$ ( $10^{12}$ ergs/cm <sup>3</sup> )	1.19
	1.21 <sup>a</sup>
$C_{44}$ ( $10^{12}$ ergs/cm <sup>3</sup> )	0.459
	0.444 <sup>a</sup>
$E_v^f$ (eV)	2.22
	2.2 <sup>c</sup>
$E_{\text{bcc}} - E_{\text{fcc}}$ (eV/atom)	0.035
$E_{\text{DBE}}$ (eV)	6.12
	2.49 <sup>d</sup>
$R_e$ (Å)	2.52
	1.77 <sup>d</sup>

<sup>a</sup>Reference 36.

<sup>b</sup>Reference 37.

<sup>c</sup>Reference 38.

<sup>d</sup>Reference 39.

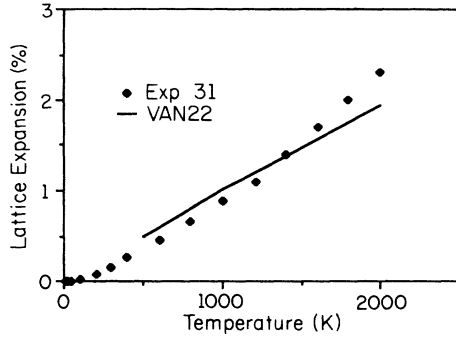


FIG. 5. Thermal expansion of vanadium. The points represent experimental data (Ref. 40), and the solid lines represent classical MC calculations with  $F^{\text{VAN}}$ . The MC results are normalized to  $a_{\text{OH}}^{0\text{K}}$ , which guarantees that the theoretical and experimental results agree at 0 K.

mental curve shows a slight upwards curvature, especially at high temperatures. This curvature is related to the fourth derivative of the potential, which appears to be incorrect. However, the overall magnitude of the thermal expansion is within 20% of experiment, which is a large improvement over the FS potentials.<sup>32</sup>

### B. Monovacancy properties

Monovacancy formation energies have been determined from positron-annihilation studies<sup>38,41</sup> and their values are listed in Table III. Migration energies may be determined from measurements of self-diffusion, as will be discussed below.

In many bcc metals (including vanadium), diffusion by monovacancies appears to be the major diffusion mechanism at moderate temperatures ( $0.5T_{\text{mp}} < T < 0.8T_{\text{mp}}$ ). The diffusion rate is given by

$$D = D_{1v}^0 \exp(-Q_{1v}/kT),$$

where  $D_{1v}^0$  is a constant, and  $Q_{1v}$  is the activation energies, given by

$$Q_{1v} = E_{1v}^f + E_{1v}^m,$$

where the  $E_{1v}^f$  is the formation energy and the  $E_{1v}^m$  is the migration energies for monovacancies.

The values of  $E_{1v}^f$  and  $Q_{1v}$  are listed in Table III; we chose to fit  $E_{1v}^f = 2.2$  eV, and  $Q_{1v} = 3.2$  eV; this yields  $E_{1v}^m = 1.0$  eV. This migration energy is consistent with the minimum temperature required for vacancy migration, 430 K.<sup>41</sup> It should be noted that the limit of experimental accuracy is approximately a couple tenths of an eV for both values (see Table III). We chose the upper range of values for  $Q_{1v}$ , since those values seem to be most consistent with the positron-annihilation data. As stated in the previous section,  $E_{1v}^f$  is directly included in the fitting procedure used to generate the functions. Then, of the functions generated, we chose the one which had the best agreement with  $E_{1v}^m$  and the thermal expansion data. The values for  $E_{1v}^f$ ,  $E_{1v}^m$ , and  $Q_{1v}$  using the FS potentials are also listed in Table III. These values are seen to be somewhat lower than the experimental values.

There has been speculation<sup>50</sup> that at high temperatures may also diffuse by jumping to next-nearest-neighbor sites (see Sec. III E). Therefore, we calculated the activation energy for the jump, and found it to be

$$E_v^{m(\text{NNN})} = 2.99 \text{ eV},$$

yielding a total self-diffusion energy of

$$Q_{1v}^{\text{NNN}} = E_v^f + E_v^{m(\text{NNN})} = 5.13 \text{ eV}.$$

This mechanism will be discussed further in Sec. III E.

TABLE III. Predicted monovacancy properties (in eV). PA are positron-annihilation experiments, and Diff. are diffusion experiments. The diffusion results are for the low-temperature regime, which probably corresponds to a monovacancy mechanism.

Ref.	$E_v^f$	$E_v^m$	$Q_v$	$E_v^{m(\text{NNN})}$	$Q_v^{(\text{NNN})}$
VAN	2.22	0.98	3.20	2.91	5.13
FS (Refs. 28,29)	1.83	0.72	2.55		
FS (Ref. 27)	1.83	0.76	2.58		
PA (Ref. 41)	2.1±0.2	1.3±0.3 <sup>a</sup>			
PA (Ref. 38)	2.2±0.4	1.2±0.3 <sup>a</sup>			
Diff. (Ref. 42)			3.20		
Diff. (Ref. 43)			3.20		
Diff. (Ref. 44)			3.21		
Diff. (Ref. 45)			3.14		
Diff. (Ref. 46)			2.82		
Diff. (Ref. 47)			2.80 <sup>b</sup>		
Diff. (Ref. 48)			2.65 <sup>b</sup>		
Diff. (Ref. 49)			3.09 <sup>c</sup>		

<sup>a</sup>Determined from PA and diffusion experiments.

<sup>b</sup>Significant impurity contamination (Ref. 49).

<sup>c</sup>Nonstandard nuclear-magnetic-resonance techniques used.

TABLE IV. Predicted divacancy formation and binding energies (in eV).

Configuration	Formation energy	Binding energy
First-nearest neighbors	3.99	0.45
Second-nearest neighbors	4.21	0.23
Third-nearest neighbors	4.50	-0.06
Fourth-nearest neighbors	4.44	0.00
Fifth-nearest neighbors	4.44	0.00

### C. Divacancy properties

The stability of several possible divacancy structures were investigated, and the nearest-neighbor divacancy was found to be the most stable (see Table IV), with a binding energy of 0.45 eV. These values contrast with calculations by Johnson using pair potentials for Fe, in which he found the second-nearest-neighbor configuration to be the most stable.<sup>50</sup>

Divacancy diffusion in bcc metals is much different than in fcc metals, due to the different positions of nearest neighbors. Specifically, in a fcc lattice there exist atoms which are nearest neighbors to both vacancies; however, this is not the case in bcc lattices. Thus, in fcc lattices a divacancy may diffuse by one of the vacancies exchanging positions with a mutual nearest neighbor, resulting in a nearest-neighbor divacancy. However, such a mechanism is not possible in bcc lattices; the divacancy must migrate either by a one-step next-nearest-neighbor (NNN) jump (to reform a nearest-neighbor divacancy) or by a two-step jump, first to an intermediate metastable configuration (see Fig. 6) and then to reform a nearest-neighbor divacancy. The activation energies for these

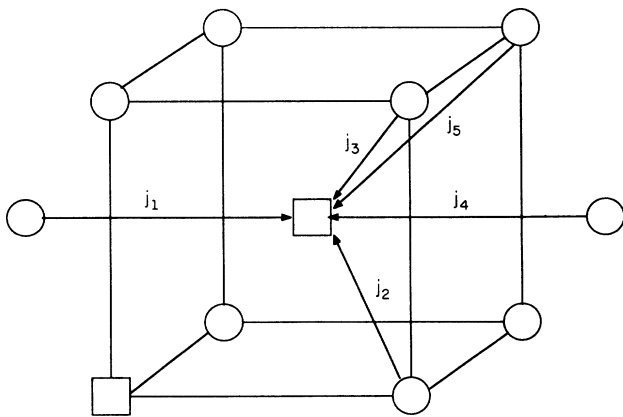


FIG. 6. Divacancy in a bcc lattice. The circles represent atoms, and the squares represent the two vacancies of a first-nearest-neighbor (NN) divacancy. The arrows indicate atomic jumps which result in migration of the divacancy. The number associated with the jump refers to the final configuration of the divacancy: first-nearest neighbor ( $j_1$ ), second-nearest neighbor ( $j_2$ ), etc. The formation energies and migration energies are listed in Tables IV and V.

TABLE V. Predicted divacancy migration energies, as calculated for one vacancy of a nearest-neighbor divacancy to migrate to a new position relative to the stationary vacancy.

Jump (see Fig. 6)	Activation energy (in eV)
$j_1$	2.47
$j_2$	1.27
$j_3$	1.24
$j_4$	2.99
$j_5$	0.97

mechanisms have been calculated, and the results are shown in Table V.

The activation energies for the migration of one vacancy (of a nearest-neighbor divacancy) are seen to depend dramatically on the migration path. The activation energy for jumps  $j_1$  and  $j_4$  are high because the vacancy migrates to a site which is a second-nearest neighbor of its first site. The other jumps ( $j_2, j_3, j_5$ ) have a much lower barrier because the vacancy migrates to a site which is a nearest neighbor to its original site. It is interesting to note that although jump  $j_5$  results in a relatively unfavorable metastable state, its migration path has the lowest activation energy. Thus, the linear migration path of jump  $j_5$  appears to be the most favorable, although jumps  $j_2$  and  $j_3$  are also expected to be significant.

It is interesting to note that unlike fcc metals where  $E_{2v}^m < E_{1v}^m$  we instead find that for bcc metals  $E_{2v}^m > E_{1v}^m$ . This is due to the fact that the divacancy must migrate via a metastable configuration in which the nearest-neighbor divacancy must split into a second-, third-, fifth-nearest-neighbor divacancy.

The activation energy for diffusion by a divacancy mechanism is  $Q_{2v} = Q_{2v}^f + Q_{2v}^m$ . The lower range of values of  $Q_{2v}$  varied from 4.96 to 5.26 eV (see Table V). This mechanism will be discussed further in Sec. III E.

### D. Self-interstitial properties

Only one fact about the properties of self-interstitials in vanadium is known, namely that they are highly mobile even at 4 K.<sup>51</sup> Since interstitials rapidly diffuse to sinks, no experiments have yet been carried out to determine the structure of an interstitial in vanadium. Experimental studies on fcc metals (Al, Cu, Ni) show that self-interstitials form a dumbbell pair about a lattice site, with the orientation of the dumbbell in the [100] direction.<sup>52</sup> In bcc metals, only Mo and Fe have been investigated experimentally, and in both cases the self-interstitials form a dumbbell pair along the [110] direction.<sup>52</sup>

Calculations by Johnson<sup>53</sup> using pair potentials confirmed that in bcc Fe the most stable configuration is the [110] split. Calculations by Rebonato *et al.*<sup>27</sup> using their modified FS potentials found that the [110] configuration is favored in Mo, Nb, and V, but in Ta the [111] configuration is more stable. Similar calculations by Ackland and Thetford<sup>30</sup> using their modified FS potentials found that the [110] configuration was most stable in V, Nb, and Ta; a bent [110] configuration was

found for Mo, and the crowdion configuration was found for W. It should be noted that the FS values of  $E_i^f$  differed by up to 1.4 eV, indicating that  $E_i^f$  was very sensitive to the modifications of the short-time potential.

In Table VI we list the results of our calculations on the formation energy of self-interstitials in vanadium. All of our calculations involved cubic systems containing 1025 atoms; systems twice as large yielded equivalent formation energies to within 0.01 eV. Surprisingly, we found that the [100] dumbbell is the most stable by a few tenths of an eV, in contrast to the experimental results for Mo and Fe. Although it is possible that the predicted results are incorrect, it is important to remember that the activation temperature for diffusion in Mo (40 K) and Fe (100 K) is over an order of magnitude higher than that for vanadium ( $< 4$  K).<sup>52</sup> This difference in the activation temperature suggests that they might have different structures.

To further test the reliability of the vanadium function, we calculated the migration energy for a [110] dumbbell, and found that during the migration it reverted to a [100] dumbbell. For the [100] dumbbell, the lowest-energy migration path is the [100] direction through the octahedral site; the migration energy is 0.06 eV, in reasonable agreement with experiment [ $< 0.01$  eV (Ref. 51)] in that both results are small. Our low value of the activation energy is further evidence of the reliability of the model, and suggests that the [100] dumbbell may in fact be the most stable configuration in vanadium.

At high temperatures, diffusion by a dissociative mechanism may be important. The dissociative mechanism involves the motion of a lattice atom into an interstitial site, leaving behind a vacancy. The interstitial atom then hops rapidly from one interstitial site to another, until it encounters a vacancy, which it enters to again become a lattice atom. Thus, the distance the interstitial diffuses is proportional to the vacancy concentration. The total activation energy for a dissociative diffusion mechanism is given by

$$Q_{\text{dis}} = E_{\text{int}}^f + E_{\text{int}}^m = 4.58 + 0.06 \text{ eV} = 4.64 \text{ eV}.$$

The vacancy-formation energy does not affect this result,<sup>12</sup> because it affects both the barrier to the creation of

a Frenkel pair and the distance the interstitial diffuses before being “trapped” by a vacancy, and these two terms exactly offset one another. This mechanism will be discussed further in the next section.

### E. High-temperature-diffusion mechanism

As discussed above, at moderate temperatures diffusion in vanadium is dominated by a vacancy mechanism. However, at high temperatures ( $> \sim 0.8T_{\text{mp}}$ ) a second mechanism dramatically increases the diffusion rate. The nature of this mechanism is unknown, but several possibilities have been suggested, namely divacancies, next-nearest-neighbor vacancy jumps, and interstitials.

In fcc metals, the high-temperature mechanism is attributed to divacancies. However, in bcc metals divacancies diffuse by a different mechanism, where  $E_{2v}^m > E_{1v}^m$ , which is the reverse of the behavior in fcc metals. Also, bcc lattices are less closely packed than fcc lattices, suggesting that self-interstitials would form more easily in bcc and fcc lattices. These two arguments suggest that bcc lattices would favor a dissociative mechanism more than a divacancy mechanism.

In Secs. III B–III D we calculated the activation energies for these migration mechanisms, and we summarize the results in Table VII. We find that the dissociative mechanism does in fact have the lowest activation energy by 0.3 eV, suggesting that it is the dominant diffusion mechanism.

Many experimental estimates of the activation energy of the high-temperature mechanism have been made from diffusion measurements; these values are listed in Table VII. The values are seen to range from 4.12 to 4.81 eV,

TABLE VII. Comparison of theoretical and experimental activation energies for a high-temperature diffusion mechanism. The results of  $F^{\text{VAN}}$  suggest that the dissociative (interstitial) diffusion mechanism is dominant, and the activation energy is in reasonable agreement with most experiments (range of 4.5–4.8 eV). Diff. means the results of diffusion experiments, which were analyzed to determine the contributions of both a low-temperature and a high-temperature mechanism. The asterisk denotes significant impurity contamination.

Ref.	Diffusion mechanism	Activation energy (in eV)
$F^{\text{VAN}}$	NNN monovacancy	5.13
	divacancy	4.96–5.26
	dissociative	4.64
FS (Ref. 27)	dissociative	3.23
FS (Ref. 30)	dissociative	4.14
Diff. (Ref. 43)	QHT	4.71
Diff. (Ref. 45)	QHT	4.81
Diff. (Ref. 46)	QHT	4.57
Diff. (Ref. 67)	QHT	4.74
Diff. (Ref. 44)	QHT	4.24
Diff. (Ref. 47)	QHT	4.48*
Diff. (Ref. 18)	QHT	4.48*

TABLE VI. Calculated interstitial properties using  $F^{\text{VAN}}$ . The formation energy is the energy required to form a Frenkel pair minus the vacancy-formation energy.

Interstitial structure	$S_{\text{SI}}^f$	$E_{\text{SI}}^m$
Split [100]	4.58	0.06 <sup>b</sup>
Split [110]	4.90	c
Split [111]	4.78	
Octahedral	4.64	
Tetrahedral	a	

<sup>a</sup>Unstable; reverts to split [100].

<sup>b</sup>Migration path is in the [100] direction to an octahedral site, which is marginally metastable.

<sup>c</sup>Unstable; during migration it reverts to a [100] configuration.

with most of the analyses in the range of 4.5–4.8 eV. This range is in excellent agreement with our calculation of  $Q_{\text{dis}} = 4.64$  eV.

The FS potentials have not yet been used to calculate the interstitial migration energy, but if we use the experi-

mental value ( $< 0.01$  eV), then  $Q_{\text{dis}}$  is found to be 3.23 (Ref. 27) or 4.14.<sup>30</sup> Although these values are rather low, they also suggest that the dissociative mechanism is the dominant high-temperature diffusion mechanism.

In summary, a comparison of activation enthalpies

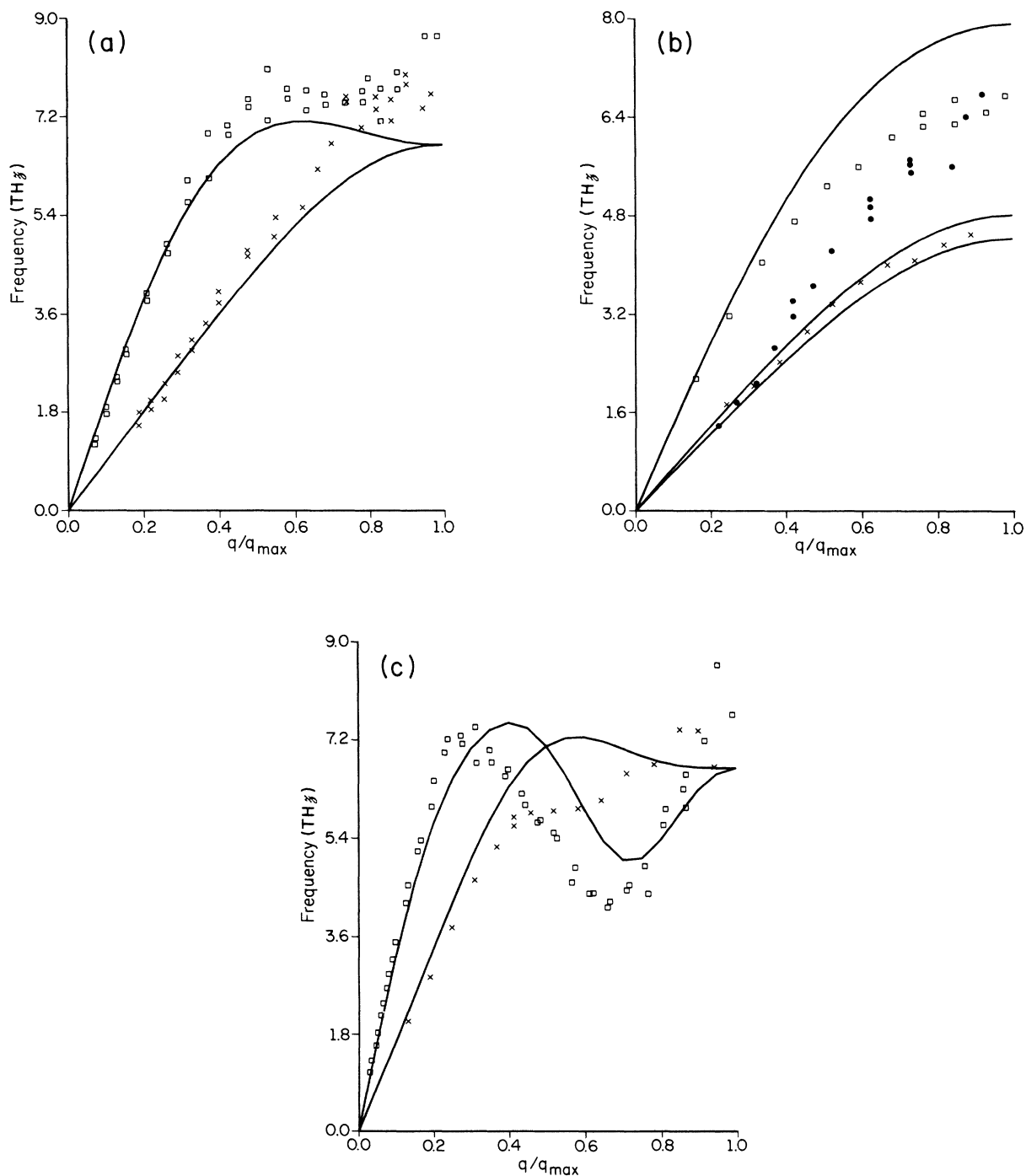


FIG. 7. Comparison of experimental (Ref. 54) and theoretical phonon dispersion in the (a) [100] direction, (b) [110] direction, and (c) [111] direction.  $q_{\text{max}}$  is  $2\pi/a$  in the [100] and [111] directions, and  $\pi/a$  in the [110] direction. The frequency is in units of THz. The points are experimental data and the lines are the calculated data.

shows that the dissociative mechanism is favored over both the divacancy and next-nearest-neighbor vacancy mechanisms. Ideally one would also like to know the formation entropy of interstitials and divacancies, but to our knowledge this has not yet been calculated for bcc metals. We have previously calculated the formation entropy of an interstitial in Cu using QH techniques, finding  $S_{\text{int}}^f = 8.4k_B$ ; this strongly suggests that a dissociative mechanism could significantly contribute to self-diffusion.

### F. Phonon dispersion

Using the same approach as Daw and Hatcher,<sup>11</sup> we calculated the phonon-dispersion curves for  $F^{\text{VAN}}$ . The results are shown in Fig. 7, and the agreement with experiment<sup>54</sup> is reasonable. In the long-wavelength limit (low  $k$ ), the dispersion curves are directly related to the elastic constants, to which the functions were fit. However, even in the short-wavelength limit the results agree with experiment to within 25%.

It should be noted that Rebonato and Broughton<sup>26</sup> used the FS potentials to calculate phonon-dispersion curves for several bcc transition metals, including vanadium, and found generally good agreement with experiment. However, they appear to have misunderstood the labeling of the experimental results for vanadium in the [110] direction, so that the experimental results are incorrectly plotted in their Fig. 4. Their results are somewhat more accurate in the [111] direction, whereas our calculations are more accurate in the [100] and [110] directions.

### G. Surface properties

We have calculated the surface energy of the (100) and (110) faces of vanadium by creating a 30-Å-thick slab with two free surfaces, and allowing the surfaces to relax. No attempt was made to search for reconstructed surfaces. The results are shown in Table VIII, and are seen to closely agree with previous FS results.<sup>55</sup> Also shown in Table VIII are Tyson's estimates of the surface energy of an "average" face, which are based on measurements of the liquid-vapor surface energy.<sup>56,57</sup> Using Tyson's estimate of the surface energy of an "average" face, and using his estimate of the "population density factor,"<sup>56,57</sup> we can also estimate the surface energy of a particular face; these results are also included in Table VIII.

Our results qualitatively agree with Tyson's, in that the (100) face has a higher surface energy than the (110) face.

TABLE VIII. Comparison of surface energies (in ergs/cm<sup>2</sup>) at 0 K.

Surface	VAN	FS (Ref. 55)	Expt.
(100)	1700	1733	2589 <sup>a</sup>
(110)	1460	1473	1822 <sup>a</sup>
Average solid			2622 <sup>b</sup>

<sup>a</sup>Our estimate using Tyson's method (Refs. 56 and 57).

<sup>b</sup>Tyson's estimate from liquid-surface energy data (Refs. 56 and 57).

TABLE IX. Surface relaxations;  $\Delta_{12}$  and  $\Delta_{23}$  are the first- and second-layer relaxations, respectively.

	Bulk value	$\Delta_{12}$	$\Delta_{23}$
(100) surface			
Expt.	(1.519 Å)	(%)	(%)
$F^{\text{VAN}}$		-6.2	+0.7
FS		-6.9	+0.3
(Ref. 55)			
LEED		-7.0	+1
(Ref. 59)			
LEED		-6.7±1.5	+1.0±1.3
(Ref. 68)			
(110) surface			
Expt.	(2.149 Å)		
$F^{\text{VAN}}$		-2.9	+0.05
FS		-3.9	+0.4
(Ref. 55)			
LEED		-0.5±0.5	
(Ref. 63)			
LEED		-0.3±0.5	
(Ref. 68)			

However, our results are only 65–80 % of the estimated value. This is consistent with previous EAM calculations, where the surface energy is approximately 75% of Tyson's estimates. The reason for this discrepancy is unclear. Ackland and Finnis<sup>55</sup> also calculated the surface energy, and their results are in close agreement with ours (see Table VIII).

Several low-energy electron diffraction (LEED) studies of vanadium surfaces have been made to determine the surface structure. These studies are complicated by the extreme difficulty of preparing a clean surface. One early study of the (100) surface found a (5×1) reconstruction,<sup>58</sup> but this seems to occur only in the presence of a significant fraction of a monolayer of oxygen.<sup>59,60</sup> Other qualitative LEED studies of the (100) (Refs. 60, 61, and 62) and (110) (Refs. 63, 64, and 65) surface found that the surface had the same 2D periodicity of the bulk planes.

Table IX compares our calculated surface relaxations with quantitative LEED studies. The overall qualitative agreement is good, in that the sign of the relaxations are always correctly predicted. The quantitative agreement for the (100) face is good for both the first-layer and second-layer relaxations. For the (110) face, we calculate a larger contraction of the first layer than is experimentally observed. We find a very small second-layer expansion; the LEED analysis did not include  $D_{23}$  as a parameter, but the accuracy of their fit suggests that  $D_{23}$  is small, in agreement with our result. It is interesting to note that our results are in fairly close agreement with those of the FS model.<sup>55</sup>

### H. Liquid density

The liquid structure was formed using MD techniques. Starting with a uniformly expanded perfect crystal of 432 atoms, the structure was annealed at 3500 K for 10 ps at constant pressure (the volume was allowed to vary). This

annealing transformed it into a liquid, which was then cooled (during 30 ps) to the melting point, 2175 K. The cooling rate was such that the volume had a sufficient time to equilibrate. One further 5-ps annealing treatment at the melting point yielded the average volume, 15.8 Å<sup>3</sup>/atom. After rescaling by  $a_{\text{OH}}^0/a_{\text{MD}}^0$  (see Sec. III B), the volume is found to be 15.6 Å<sup>3</sup>/atom, in reasonable agreement with the experimental value of 15.2 Å<sup>3</sup>/atom.<sup>66</sup>

A word of warning should be added about this calculation, however. After the liquid was equilibrated at 2175 K, its structure factor was calculated<sup>5</sup> and resembled that of an amorphous solid in that the amplitude of the structure factor was larger than that usually seen for liquids, and the second maximum in the pair-correlation function had a double-peak structure. Thus it is possible that this structure was an amorphous solid rather than a liquid. This suggests that the melting point of  $F^{\text{VAN}}$  is somewhat higher than experiment. Further calculations are required.

#### IV. SUMMARY

In summary, we have presented the determination of  $F^{\text{VAN}}$ , an EAM function for vanadium. It was developed by directly fitting the lattice constant, sublimation energy, elastic constants, and vacancy-formation energy, and by indirectly fitting the thermal expansion and vacancy migration energy. The fit to those quantities was accurate to within 3%, except for thermal expansion, which was accurate to about 20%. This agreement for vacancy properties and especially thermal expansion is a large improvement over the FS potentials.

$F^{\text{VAN}}$  was also used to calculate the following.

(1) Vacancy-migration energy by a next-nearest-neighbor mechanism. The high value of  $E_{1v}^{m(\text{NNN})}$  (2.91 eV) suggest that this is not a significant diffusion mechanism.

(2) Divacancy formation and migration energies. Nearest-neighbor divacancies were found to be the most stable, but divacancy diffusion occurs via a metastable configuration. The high values of  $Q_{2v}$  (4.96–5.26 eV) suggest that this is not a significant diffusion mechanism.

(3) Interstitial structure and migration energy. The most stable interstitial structure was found to be the [100] split dumbbell, in contrast to the FS model which predicted the [110] split. The migration energy was found to be 0.06 eV, in reasonable agreement with the experimental value (<0.01 eV). The combined formation and migration energy is  $Q_{\text{int}}$ , the activation energy for a dissociative diffusion mechanism; the relatively low value of 4.64 eV strongly suggests that this is the dominant high-temperature mechanism. Furthermore, this value is in excellent agreement with experimental measurements of the activation energy (4.5–4.8 eV).

(4) Phonon dispersion. Phonon dispersion in the [100], [110], and [111] directions is in good agreement with experiment in the long-wavelength limit, and even in the short-wavelength limit the results agree with experiment to within 25%.

(5) Surface energy and relaxation. The surface energy

is found to be about 75% of experimental estimates, consistent with other EAM calculations.<sup>4</sup> The calculated surface relaxations of the first and second layers of the (100) and (110) surface are in reasonable agreement with LEED measurements.

(6) Liquid volume. The volume of the liquid at the melting point was found to be 15.6 Å<sup>3</sup>/atom, in good agreement with the experimental value of 15.2 Å<sup>3</sup>/atom. However, it is possible that the liquid was in fact a disordered solid.

In summary, this potential fairly accurately describes a wide range of material properties, although the phonon-dispersion and liquid-volume results suggest that further improvement could be made. The accuracy of this potential is presumably due to including thermal expansion and vacancy migration in the fit. Whereas the elastic constants are related to the second derivatives of the potential, thermal expansion is related to the third derivative. Similarly, vacancy migration tests the potential far from equilibrium, so that including it in the fit also increases the reliability of the potential.

The importance of the form of the cutoff suggests that the simple Morse potential used for the electrostatic interaction should be replaced with a more general form (see Johnson and Oh<sup>33</sup>), which might result in even more accurate potentials for the bcc metals.

#### ACKNOWLEDGMENTS

We especially thank Dr. Art Voter of Los Alamos National Laboratories for sharing his unpublished results

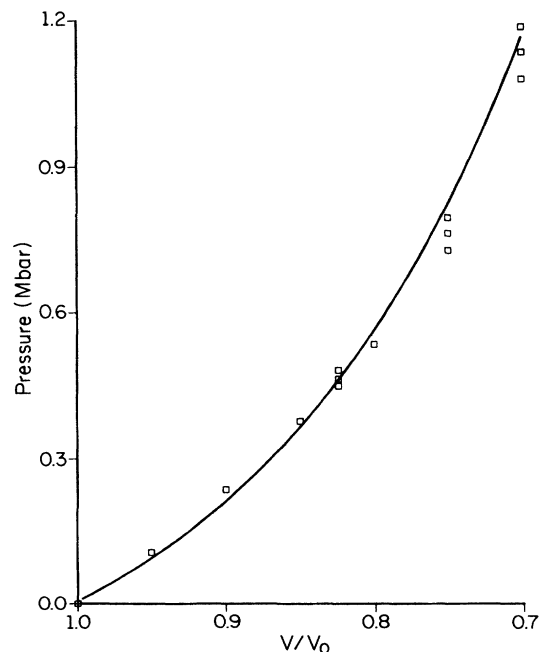


FIG. 8. Pressure vs volume relation for the universal cohesive energy relation (Ref. 31), as compared with experimental data (Ref. 27). Error bars included on the experimental data where appropriate. This figure corrects earlier calculations (Ref. 27).

with us, as well as for his useful comments and suggestions. We would also like to thank the following people for their helpful comments and suggestions: Dr. Murray Daw, Dr. Jeff Nelson, Dr. Mike Baskes, Dr. Tom Felner, and Dr. Bill Wolfer of Sandia National Laboratories–Livermore, Dr. Graham Ackland of the University of Pennsylvania, and Dr. Gerhard Neumann of the Freie Universität Berlin. This work was supported by the U.S. Department of Energy (Division of Materials Science of the Office of Basic Energy Sciences).

**APPENDIX: PRESSURE VERSUS VOLUME  
RELATION FOR THE UNIVERSAL COHESIVE  
ENERGY RELATION (REF. 31)**

The universal cohesive energy relation was developed by Rose *et al.*,<sup>31</sup> and several sets of EAM functions (including  $F^{\text{VAN}}$ ) have been developed which require an exact fit to it. For uniform distortions of the lattice constant, the cohesive energy of each atom is given by  $U$ :

$$U = -E_{\text{sub}}(1+a^*)\exp(-a^*), \quad (\text{A1})$$

where  $a^*$  is given by

$$a^* = (a/a_0 - 1)/(E_{\text{sub}}/9B\Omega)^{1/2}. \quad (\text{A2})$$

$E_{\text{sub}}$  is the sublimation energy at 0 K,  $a$  is the distorted lattice constant,  $a_0$  is the equilibrium lattice constant at 0 K,  $B$  is the bulk modulus, and  $\Omega$  is the atomic volume at 0 K.

The pressure versus volume relation can be determined from

$$P = -dU/dV, \quad (\text{A3})$$

and in Fig. 8, we plot the result for vanadium, using the values in Table II. We also compare with the averaged experimental data, as determined by Rebonato *et al.*<sup>27</sup> In contrast with an earlier calculation which probably contained an error,<sup>27</sup> we find that the calculated pressure versus volume relation is in excellent agreement with experiment over the entire range.

Present address: Department of Materials Science, University of Illinois at Urbana-Champaign, 104 South Goodwin Avenue, Urbana, IL 61801.

- <sup>1</sup>M. S. Daw and M. I. Baskes, *Phys. Rev. B* **29**, 6443 (1984).  
<sup>2</sup>M. S. Daw, *Phys. Rev. B* **39**, 7441 (1989).  
<sup>3</sup>K. W. Jacobsen, J. K. Nørskov, and M. J. Puska, *Phys. Rev. B* **35**, 7423 (1987).  
<sup>4</sup>S. M. Foiles, M. I. Baskes, and M. S. Daw, *Phys. Rev. B* **33**, 7983 (1986).  
<sup>5</sup>S. M. Foiles, *Phys. Rev. B* **32**, 3409 (1985).  
<sup>6</sup>J. B. Adams, S. M. Foiles, and W. G. Wolfer, *J. Mater. Res.* **4**, 102 (1989).  
<sup>7</sup>S. M. Foiles, *Phys. Rev. B* **32**, 7685 (1985).  
<sup>8</sup>A. F. Voter and S. P. Chen, in *Mater. Res. Soc. Symp. Proc.* **82**, 175 (1987).  
<sup>9</sup>F. Ercolessi, E. Tosatti, and M. Parrinello, *Phys. Rev. Lett.* **57**, 719 (1986).  
<sup>10</sup>D. J. Oh and R. A. Johnson, *J. Mater. Res.* **3**, 471 (1988).  
<sup>11</sup>M. S. Daw and R. D. Hatcher, *Solid State Commun.* **56**, 697 (1985).  
<sup>12</sup>J. B. Adams and W. G. Wolfer, *J. Nucl. Mater.* **158**, 25 (1988).  
<sup>13</sup>S. M. Foiles and J. B. Adams, *Phys. Rev. B* **40**, 5909 (1989).  
<sup>14</sup>S. M. Foiles and M. S. Daw, *Phys. Rev. B* **38**, 12643 (1988).  
<sup>15</sup>S. M. Foiles, M. I. Baskes, and M. S. Daw, in *Interfacial Structure, Properties, and Design*, edited by M. H. Yoo, W. A. T. Clark, and C. L. Briant (MRS, Pittsburgh, 1988), p.343.  
<sup>16</sup>S. M. Foiles and J. B. Adams, *Phys. Rev. B* **40**, 5909 (1989).  
<sup>17</sup>B. W. Dodson, *Phys. Rev. B* **35**, 880 (1987).  
<sup>18</sup>M. S. Daw and S. M. Foiles, *Phys. Rev. Lett.* **59**, 2756 (1987).  
<sup>19</sup>S. M. Foiles, in *Surface Segregation and Related Phenomena*, edited by P. A. Dowben and A. Miller (Chemical Rubber Co., Cleveland, in press).  
<sup>20</sup>J. S. Nelson, M. S. Daw, and E. C. Sowa, *Phys. Rev. B* **40**, 1465 (1989).  
<sup>21</sup>J. S. Nelson, E. C. Sowa, and M. S. Daw, *Phys. Rev. Lett.* **61**, 1977 (1988).  
<sup>22</sup>S. P. Chen, D. J. Srolovitz, and A. F. Voter, *J. Mater. Res.* **4**, 62 (1989).  
<sup>23</sup>M. I. Baskes, *Phys. Rev. Lett.* **59**, 2666 (1987).  
<sup>24</sup>M. I. Baskes, J. S. Nelson, and A. F. Wright, *Phys. Rev. B* **40**, 6085 (1989).  
<sup>25</sup>M. W. Finnis and J. E. Sinclair, *Philos. Mag. A* **50**, 45 (1984).  
<sup>26</sup>R. Rebonato and J. Q. Broughton, *Philos. Mag. Lett.* **55**, 225 (1987).  
<sup>27</sup>R. Rebonato, D. O. Welch, R. D. Hatcher, and J. C. Billelo, *Philos. Mag. A* **55**, 655 (1987).  
<sup>28</sup>J. M. Harder and D. J. Bacon, *Philos. Mag. A* **54**, 651 (1987).  
<sup>29</sup>C. C. Matthai and D. J. Bacon, *Philos. Mag. A* **52**, 1 (1985).  
<sup>30</sup>G. J. Ackland and R. Thetford, *Philos. Mag. A* **56**, 15 (1987).  
<sup>31</sup>J. H. Rose, J. R. Smith, F. Guinea, and J. Ferrante, *Phys. Rev. B* **29**, 2963 (1984).  
<sup>32</sup>M. Marchese, G. Jacucci, and C. P. Flynn, *Philos. Mag. Lett.* **57**, 25 (1988).  
<sup>33</sup>R. A. Johnson and D. J. Oh (unpublished).  
<sup>34</sup>J. Eridon and S. Rao, *Philos. Mag. Lett.* **59**, 31 (1989).  
<sup>35</sup>J. Nelson (private communication).  
<sup>36</sup>G. Simmons and H. Wang, *Single Crystal Elastic Constants and Calculated Aggregate Properties: A Handbook*, 2nd ed. (MIT Press, Cambridge, Mass., 1971).  
<sup>37</sup>C. Kittel, *Introduction to Solid State Physics*, 5th ed. (Wiley, New York, 1976).  
<sup>38</sup>C. Janot, B. George, and P. Delcroix, *J. Phys. F* **12**, 47 (1982).  
<sup>39</sup>M. D. Morse, *Chem. Rev.* **86**, 1049 (1986).  
<sup>40</sup>Y. S. Touloukian, R. K. Kirby, and R. E. Taylor, *Thermophysical Properties of Matter: Thermal Expansion of Metallic Elements and Alloys* (Plenum, New York, 1975), Vol. 12.  
<sup>41</sup>K. Maier, M. Peo, B. Saile, H. E. Schaefer, and A. Seeger, *Philos. Mag. A* **40**, 701 (1979).  
<sup>42</sup>G. M. Neumann, in *Diffusion Processes*, edited by J. N. Sherwood, A. V. Chadwick, W. M. Muir, and F. L. Swinton (Gordon and Breach, London, 1971), p. 329.  
<sup>43</sup>R. F. Peart, *J. Phys. Chem. Solids* **26**, 1853 (1965).  
<sup>44</sup>J. Pelleg, *Philos. Mag.* **29**, 383 (1974).  
<sup>45</sup>H. M. Morrison, *Philos. Mag.* **31**, 243 (1975).  
<sup>46</sup>M.-P. Macht, G. Frohberg, and H. Wever, *Z. Metallkd.* **70**, 209 (1979).  
<sup>47</sup>R. P. Agarwala, S. P. Murarka, and M. S. Anand, *Acta Metall.* **16**, 61 (1968).  
<sup>48</sup>T. S. Lundy and C. J. McHargue, *Trans. Metall. Soc. AIME* **233**, 243 (1965).  
<sup>49</sup>B. Gunther and O. Kanert, *Acta Metall.* **31**, 909 (1983).  
<sup>50</sup>G. Neumann, *Mater. Sci. Forum* (to be published).

- <sup>51</sup>R. R. Coltman, C. E. Klabunde, J. K. Redman, and J. M. Williams, *Radiat. Eff.* **24**, 69 (1975).
- <sup>52</sup>F. W. Young, Jr., *J. Nucl. Mater.* **69/70**, 310 (1978).
- <sup>53</sup>R. A. Johnson, *Phys. Rev.* **134**, A1329 (1964).
- <sup>54</sup>R. Collella and B. W. Batterman, *Phys. Rev. B* **1**, 3913 (1970).
- <sup>55</sup>G. J. Ackland and M. W. Finnis, *Philos. Mag. A* **54**, 301 (1986).
- <sup>56</sup>W. R. Tyson, *Can. Metall. Quart.* **14**, 307 (1975).
- <sup>57</sup>W. R. Tyson and W. A. Miller, *Surf. Sci.* **62**, 267 (1977).
- <sup>58</sup>P. W. Davies and R. M. Lambers, *Surf. Sci.* **95**, 571 (1980).
- <sup>59</sup>V. Jensen, J. N. Andersen, H. B. Nielsen, and D. L. Adams, *Surf. Sci.* **116**, 66 (1982).
- <sup>60</sup>J. S. Foord, A. P. C. Reed, and R. M. Lambert, *Surf. Sci.* **129**, 79 (1983).
- <sup>61</sup>F. J. Szalkowski and G. A. Somorjai, *J. Chem. Phys.* **35**, 6097 (1972).
- <sup>62</sup>F. J. Szalkowski and G. A. Somorjai, *J. Chem. Phys.* **64**, 2985 (1976).
- <sup>63</sup>D. L. Adams and H. B. Nielsen, *Surf. Sci.* **116**, 598 (1982).
- <sup>64</sup>T. W. Haas, A. G. Jackson, and M. P. Hooker, *J. Chem. Phys.* **46**, 3025 (1967).
- <sup>65</sup>E. A. K. Nemeš and R. C. Cinti, *Surf. Sci.* **40**, 583 (1973).
- <sup>66</sup>E. T. Turkdogan, *Physical Chemistry of High Temperature Technology* (Academic, New York, 1980).
- <sup>67</sup>R. F. Peart and J. Askill, *Phys. Status Solidi* **23**, 263 (1967).
- <sup>68</sup>D. L. Adams, H. B. Nielsen, and J. N. Andersen, *Phys. Scr.* **T4**, 22 (1983).